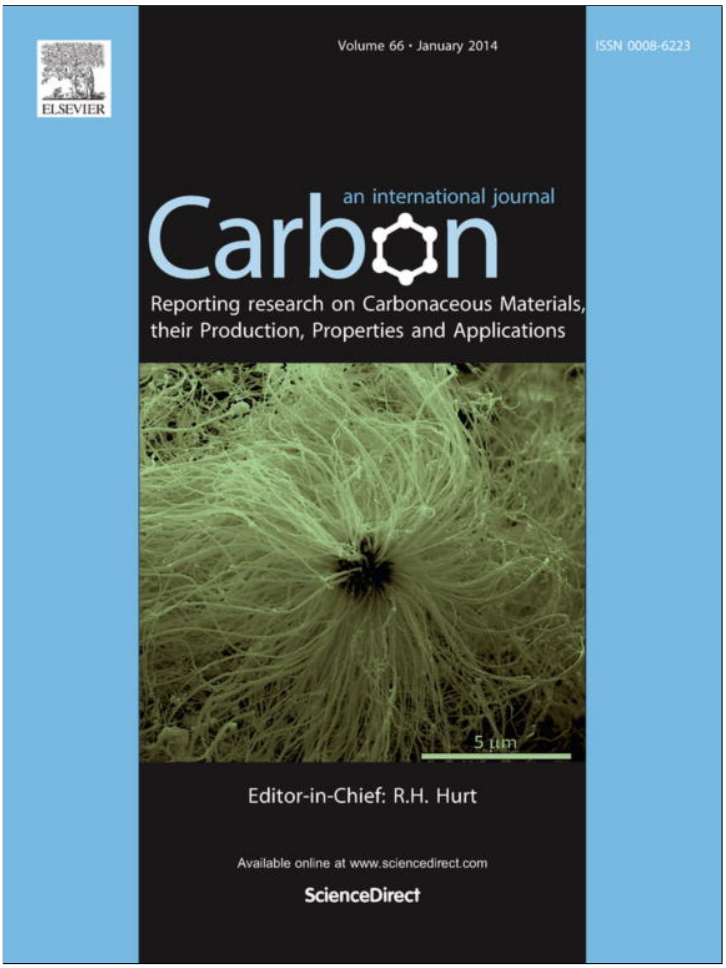

CARBON 66 (2014) 523–529

Available at www.sciencedirect.com

ScienceDirect

journal homepage: www.elsevier.com/locate/carbon

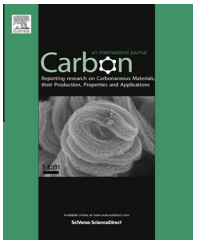

Role of cone angle on the mechanical behavior of cup-stacked carbon nanofibers studied by atomistic simulations

Jingjun Gu [a], *Frederic Sansoz* [a,b,*]

[a] *Mechanical Engineering Program, School of Engineering, The University of Vermont, Burlington, VT 05405, United States*
[b] *Materials Science Program, The University of Vermont, Burlington, VT 05405, United States*

ARTICLE INFO

Article history:
Received 26 July 2013
Accepted 8 September 2013
Available online 18 September 2013

ABSTRACT

Classical molecular dynamics simulations are used to study the effects of cone angle on mechanical properties and failure mechanisms in thermally-treated cup-stacked CNFs. We find a 22-fold reduction in elastic modulus and 4-fold decrease in tensile strength of cup-stacked CNFs with a wide range of cone angles between 19.2° and 180°. Our results show significant elastic stiffening for intermediate angles between 38.9° and 112.9°, as well as a minimum in tensile strength at a critical cone angle, due to the competition between weak van-der-Waals forces between layers and strong strengthening mechanisms from surface bonds introduced during thermal treatment. Different failure modes in CNFs subjected to tensile deformation are also predicted as a function of cone angle. This study constitutes an important step toward understanding the origin of strength dispersions observed experimentally in CNFs, and suggests that the design of high-strength CNFs can be optimized structurally by appropriately tuning the cone angle.

1. Introduction

Carbon nanofibers (CNFs) are important structural and functional materials due to excellent mechanical, electrical and chemical properties, and are more attractive than carbon nanotubes (CNTs) for high-throughput applications such as nanocomposites due to their low processing cost [1–6]. CNFs have a unique structure composed of conical graphitic layers organized in a cup-stacked morphology with hybrid characteristics of cylindrical and conical elements. Past experimental studies [7–11] have shown significant statistical variations in the elastic modulus and tensile strength of cup-stacked CNFs because large differences exist in the structure of surface and internal bonds between fibers; yet limited information at the molecular scale exists about this particular structure–property relationship [12].

Generally, four independent parameters are used to define the structure of CNFs, i.e., the length L, outer radius R, inner radius r, and cone angle θ, which only includes five possible values by symmetries of the graphene layers [13]. Although previous theoretical models using continuum mechanics theory have been proposed to predict the elastic properties of CNFs with highly-idealized structures [14,15], a predictive understanding of mechanical properties and fracture behavior based on the internal structure of CNFs has proved challenging, since the role of cone angle on surface structure and chemical bonding is difficult to verify experimentally. Here, we use classical molecular dynamics (MD) simulations to examine the role of bond structure on mechanical

* *Corresponding author at:* Mechanical Engineering Program, School of Engineering, The University of Vermont, Burlington, VT 05405, United States.
E-mail address: frederic.sansoz@uvm.edu (F. Sansoz).
0008-6223/$ - see front matter
http://dx.doi.org/10.1016/j.carbon.2013.09.029

properties in cup-stacked CNFs with a wide range of cone angles, $19.2° \leqslant \theta \leqslant 180°$, as well as in a multi-walled CNT (MWCNT) model ($\theta = 0°$) for comparison. Our results shed light on the competition between weak van-der-Waals (vdW) forces between cones and strong surface bond strengthening arising from folding of graphene bilayer edges (BLEs) introduced by thermal treatment, as well as underscore its importance for predicting the mechanical behavior and failure of CNFs as a function of cone angle.

2. Computational methods

MD simulations were performed with the software LAMMPS [16] using the AIREBO interatomic potential [17] and a modified version of this potential, which accounts for a better prediction of failure strain in C–C bonds [18,19]. Following the methodology described in our previous study [20], periodic boundary conditions were applied along the fiber axis in order to eliminate size effects that could potentially affect the strength calculation. In this study, the periodic length L, outer radius R, and inner radius r were equal to 20 nm, 3.8 nm, and 2.1 nm, respectively. Each CNF was comprised of $N = 10 \sim 60$ carbon nanocones stacked together with an interlayer distance equal to

$$\lambda = \frac{\lambda_0}{\sin\left(\frac{\theta}{2}\right)} \tag{1}$$

where λ_0 is the equilibrium distance between two graphene layers (3.4 Å). Each nanocone of angle θ and radius R was constructed by projection of a flat wedge-shaped graphene sheet of angle α and radius R' given the relations $\theta = 2\arcsin\left(\frac{\alpha}{2\pi}\right)$ and $R = \frac{\alpha R'}{2\pi}$, as schematically represented in Fig. 1. Consequently, the transformed XYZ coordinates of each atom in the cone were given by

$$X = \frac{\alpha}{2\pi}\sqrt{x^2+y^2}\cos\left[\frac{2\pi}{\alpha}\arctan\left(\frac{y}{x}\right)\right] \tag{2}$$

$$Y = \frac{\alpha}{2\pi}\sqrt{x^2+y^2}\sin\left[\frac{2\pi}{\alpha}\arctan\left(\frac{y}{x}\right)\right] \tag{3}$$

$$Z = -\sqrt{(x^2+y^2)\left[1-\left(\frac{\alpha}{2\pi}\right)^2\right]} \tag{4}$$

where x and y are the atom coordinates in the flat sheet. A hollow core of radius r was created by removing atoms inside the CNF. Fig. 2a–g display the atomistic backbone structure of CNFs created in this work and visualized using Ovito [21]. We note that all CNFs had same inner and outer radii and that those with $\theta = 0°$ and $\theta = 180°$ correspond to an armchair MWCNT and a platelet-like graphitic CNF with 60 layers, respectively.

Interlayer C–C bonds on the inner and outer free surfaces were formed by structural relaxation at high temperature under zero load using the procedure described elsewhere [20]. Here thermal treatment consisted in heating the molecular system to 2273 K at a constant rate of 24.5 K ps^{-1}, keeping the system at this temperature for 20,000 time steps, cooling it at the same rate, and equilibrating it for another 20,000 time steps. The time step was 1–2 fs. It should be emphasized that the surface bonding in our models is introduced "naturally"

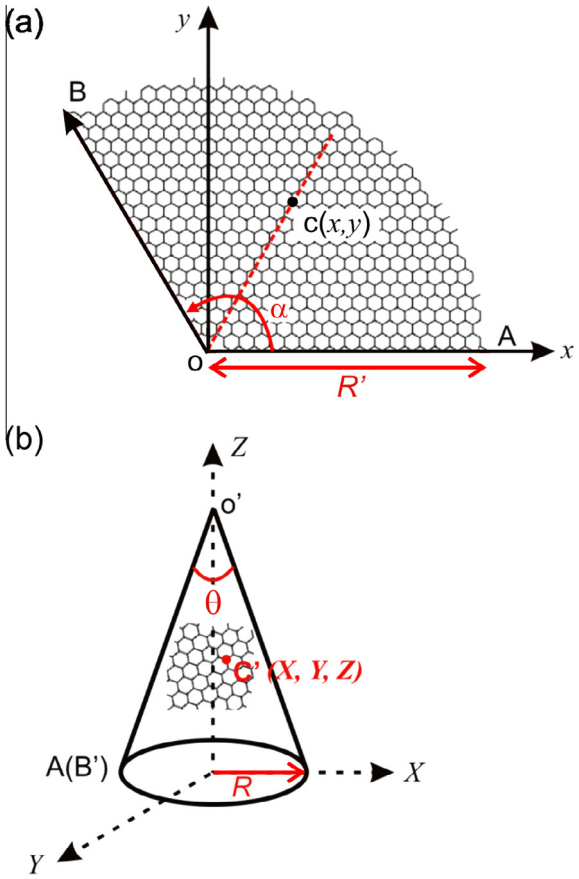

Fig. 1 – Nanocone construction. Notations used in the transformation of (a) a flat wedge-shaped graphene sheet into (b) a nanocone. (A colour version of this figure can be viewed online.)

by thermal activation rather than "by hand" using a distance criterion to force nearby C atoms to bond together as in previous atomistic studies [22,23]. This bonding scheme and the potentials used made it possible to simulate different types of covalent C–C bonds, such as sp, sp^2, and sp^3 bonds, without any pre-determined criterion and regardless of the cone angle considered.

In order to assess surface bonding quantitatively, the number of surface bonds was calculated by measuring the distance between edge atoms of adjacent cones and defining bonding when this distance was less than the sp^3 bond length = 0.154 nm. A caveat, however, is that all sp^2 bonds in the innermost and outermost walls of the MWCNT qualified as surface bonds in this approach. Therefore, owing to the armchair chirality, only bonds not perpendicular to the fiber axis were considered here. For consistency, we used the density of surface bonds f calculated by dividing the number of surface bonds by the total number of atoms present in the system, similar to previous studies [22,24] to quantitate sp^3 bridging between graphene layers.

Deformation of thermally-treated fibers was performed by subjecting the simulation box to tensile elongation at a constant engineering strain rate of 10^8 s^{-1}. Pure tension was carried out at 300 K using a constant number of particles, constant volume and constant temperature (NVT) scheme. The

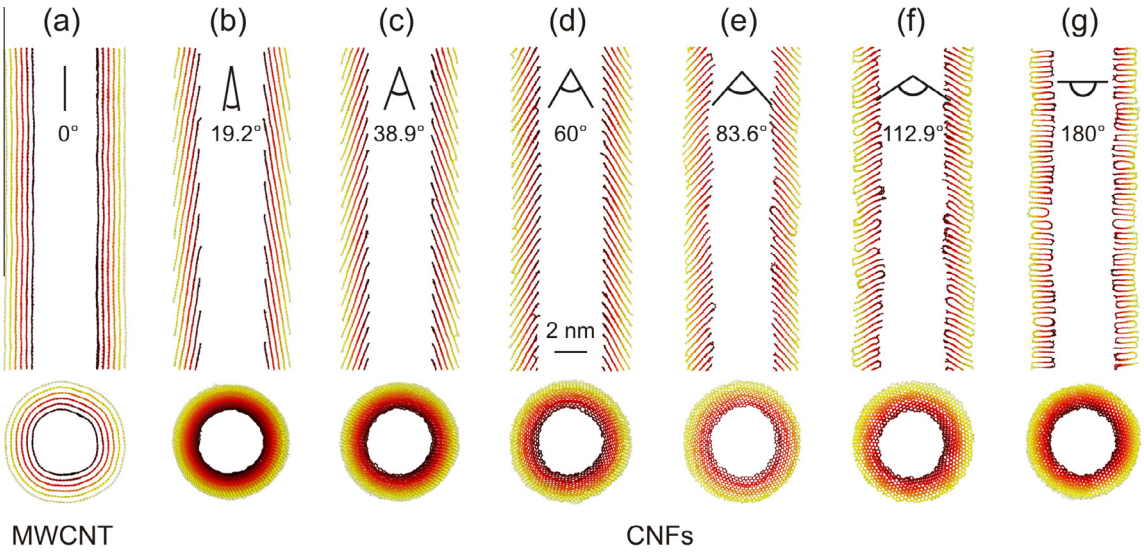

Fig. 2 – Skeletons of atomic models of cup-stacked CNFs with a cone angle θ increasing from 0° (MWCNT) to 180° (platelet-like graphitic fiber) viewed on longitudinal and transverse cross-sections. Each CNF was relaxed under zero load at 2273 K, then down to 300 K. The MWCNT was just relaxed at 300 K. (A colour version of this figure can be viewed online.)

time step was 2 fs. The true stress in the loading direction was averaged over the entire volume of the fiber using the Virial theorem.

3. Results and discussion

3.1. *Effect of cone angle on thermally-relaxed microstructures*

Fig. 3a shows the surface bonds introduced by thermal treatment between layers of a platelet-like CNFs ($\theta = 0°$). The mechanisms of surface bond formation when the cone angle is large, $\theta \geqslant 60°$, was found to be similar to those in our pre-

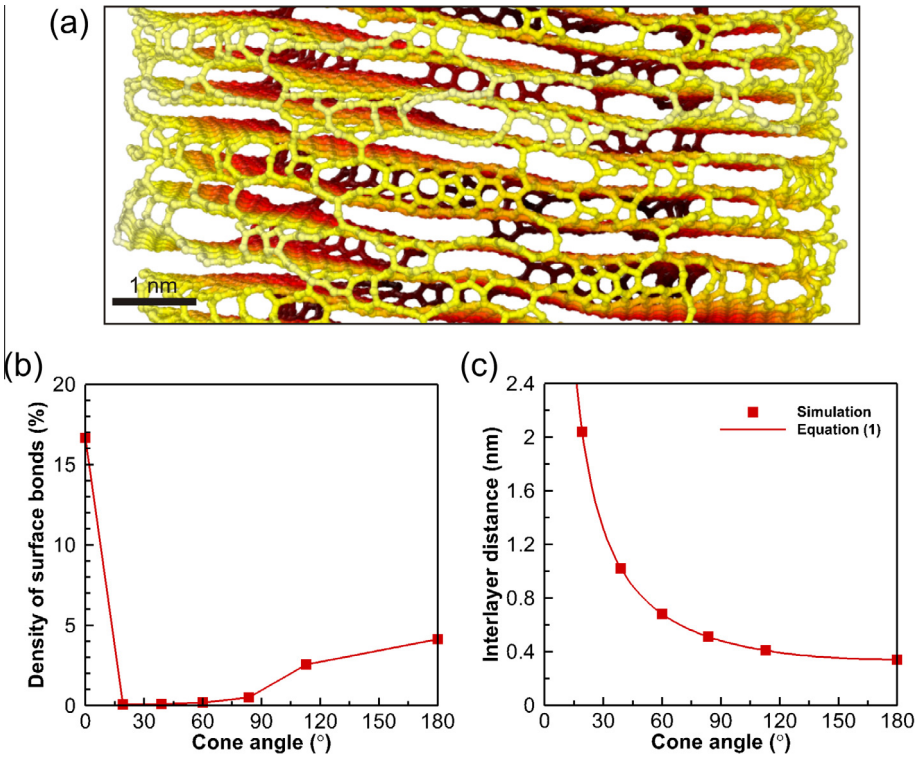

Fig. 3 – (a) Close-up view on surface bonds introduced by thermal treatment between 9 layers of a platelet-like fiber (θ = 180°). (b) Density of surface bonds as a function of θ. (c) Relation between the interlayer distance at equilibrium λ and θ from simulation and theory. (A colour version of this figure can be viewed online.)

vious study at different temperatures [20], i.e., thermal relaxation of pristine CNFs at 2273 K is accompanied by both the formation of loops from dangling bonds and the folding of BLEs in adjacent CNF layers. In contrast, however, only dangling bond loops were found to form for small cone angles, $\theta < 60^{\circ}$, suggesting that the impact of cone angle on surface bond mechanisms cannot be neglected.

Fig. 3b shows the density of surface bonds f introduced by the same thermal treatment as a function of θ. As expected, f is significantly smaller in cup-stacked CNFs than MWCNTs; however, we also find a pronounced increase of f in cup-stacked CNFs for $\theta \geqslant 60^{\circ}$. f attains up to 4.6% of the total volume of fiber with $\theta = 180^{\circ}$ in our simulations. Atomistic results in Fig. 3c and theory in Eq. (1) demonstrate that the net increase in f coincides with a decrease in interlayer distance below $\lambda = 0.68$ nm. It is known in graphite and few-layer graphene that the C sheets can fold over on themselves at the exposed ends [25–28]. The dangling bonds at the ends of a graphene sheet have such high energy that there is a strong driving force for the rapid saturation of those bonds. During typical processing of vapor-grown CNFs, one might expect foreign atoms such as H to saturate many of these dangling bonds. Although the simulated conditions envisioned here are not necessarily realistic, the folding of BLEs, which is the predominant form of bonding observed at large cone angles in our simulations, has been extensively reported in experiments. Here, increasing θ from 0° moves the exposed ends of the cones further closer and increases the bonding, until the angle approaches 180° when the graphite limit is attained.

3.2. Effect of cone angle on Young's modulus

The effects of cone angle on the elasticity of simulated CNFs is represented in Fig. 4. The axial modulus E_z is found to decrease from 754 GPa ($\theta = 0^{\circ}$) to 9.3 GPa ($\theta = 180^{\circ}$). Here, the obtained modulus in the MWCNT is in good agreement with values in the literature on SWCNTs, 1.1 TPa ~ 0.73 TPa [18,19,31], considering that the modulus of SWCNTs is predicted to decrease as the tube diameter increases. For CNFs alone, the reduction in axial modulus is 22-fold from 203 GPa to 9.3 GPa. This is consistent with past experimental measurements of Young's modulus, which have been reported to vary from 23 GPa to 245 GPa [10,11] in vapor-grown CNFs of equivalent diameters.

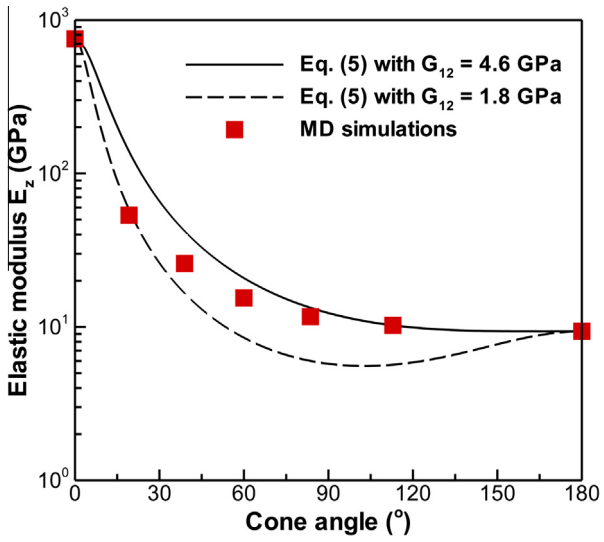

Fig. 4 – Effect of cone structure on Young's modulus in CNFs deformed in uniaxial tension. Continuum mechanics theory predictions given by Eq. (5) with different interlayer shear modulus G_{12} are shown for comparison. Significant elastic stiffening effects appear for $38.9^{\circ} \leqslant \theta \leqslant 112.9^{\circ}$. (A colour version of this figure can be viewed online.)

The poor mechanical stiffness of cup-stacked structures is clearly understood in general terms by the absence of chemical bonds between cones. The weak vdW bonding between graphitic planes is the only source of mechanical coupling, and since these bonds are very soft, the modulus of the CNF is very small relative to a CNT. This general result is somewhat identical to the steep drop in stiffness of a standard carbon–epoxy ply system, where the modulus for uniaxial loading along the fiber axis is very high, being controlled by the stiff fibers, but for loading at relatively small angles away from the fiber axis the modulus drops precipitously because it is controlled by the polymer matrix modulus, which is 100 times smaller. Thus, the present results may be viewed as the "cylindrical" version of the standard composite ply result.

To demonstrate this idea more quantitatively, Uchida et al. [15] have proposed a continuum model based on anisotropic elasticity in graphite in order to account for the variation of E_z with θ such that

$$E_z = \left[\frac{1}{E_2} + \left(\frac{1}{G_{12}} - 2\frac{\upsilon_{12}}{E_1} - \frac{2}{E_2}\right)\cos^2\left(\frac{\theta}{2}\right) + \left(\frac{1}{E_1} + \frac{1}{E_2} - \frac{1}{G_{12}} + 2\frac{\upsilon_{12}}{E_1}\right)\cos^4\left(\frac{\theta}{2}\right)\right]^{-1} \quad (5)$$

where E_1, E_2, G_{12} and υ_{12} are the longitudinal modulus, transverse modulus, interlayer shear modulus, and Poisson's ratio of graphite, respectively. Here, it is assumed $E_1 = 754$ GPa, $E_2 = 9.3$ GPa, and $\upsilon_{12} = 0.3$; however, we vary the shear modulus G_{12} because this parameter is expected to increase significantly with the amount of interlayer bonding as shown in previous studies [22,24]. The evidence presented in Fig. 4 shows that the MD simulation data are accompanied by a net increase of shear modulus from 1.8 GPa to 4.6 GPa, whereas interlayer vdW interactions provide weak resistance to shearing [29]. In particular, such elastic stiffening effect becomes significant for $38.9^{\circ} \leqslant \theta \leqslant 112.9^{\circ}$, which appears to be consistent with the increase of surface bonds in CNFs with $\theta \geqslant 60^{\circ}$. However, the effect of surface bonds on G_{12} vanishes at large θ angles because the resolved shear stress on the interlayer cancels out when $\theta = 180^{\circ}$.

3.3. Effect of cone angle on tensile strength and plastic deformation mechanisms

It is worth noting that we have used the modified AIREBO potential to enable proper bond breaking during CNF deformation. However, the stress–strain curves associated with thermally-treated cup-stacked CNFs presented in Fig. 5a were not found to be affected by the potential used. We therefore postulate that it is not important to consider bond breaking and forming in this case, and that the tensile strength corresponds to the maximum stress peak attained in the curve. In

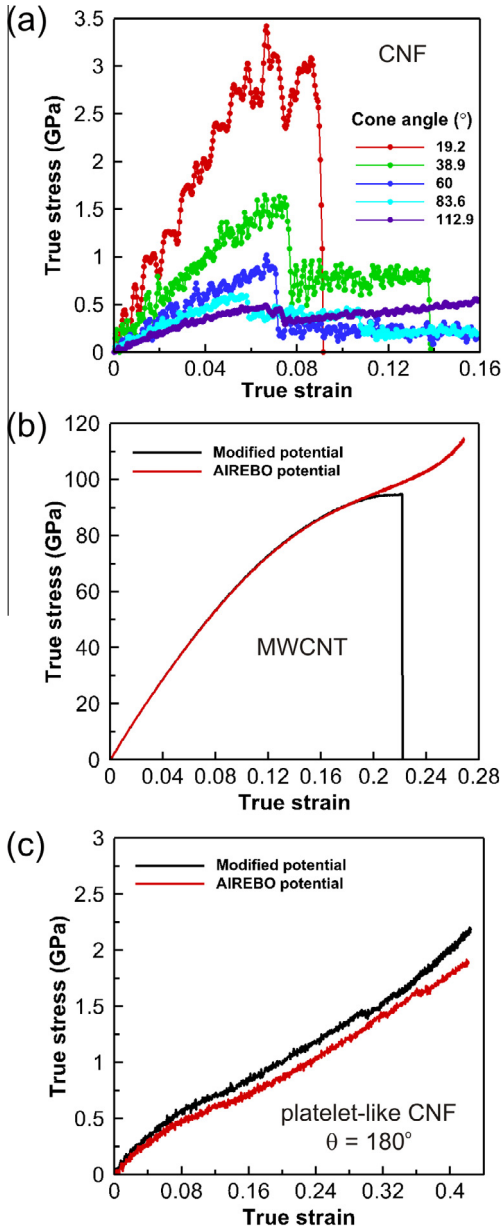

Fig. 5 – Stress–strain curves simulated at 300 K under a constant strain rate of 10^8 s^{-1} for (a) thermally-treated cup-stacked CNFs with $19.2° \leqslant \theta \leqslant 112.9°$, (b) a MWCNT ($\theta = 0°$) and (c) a thermally-treated platelet-like graphitic CNF ($\theta = 180°$) using the AIREBO potential and a modified version of this potential. (A colour version of this figure can be viewed online.)

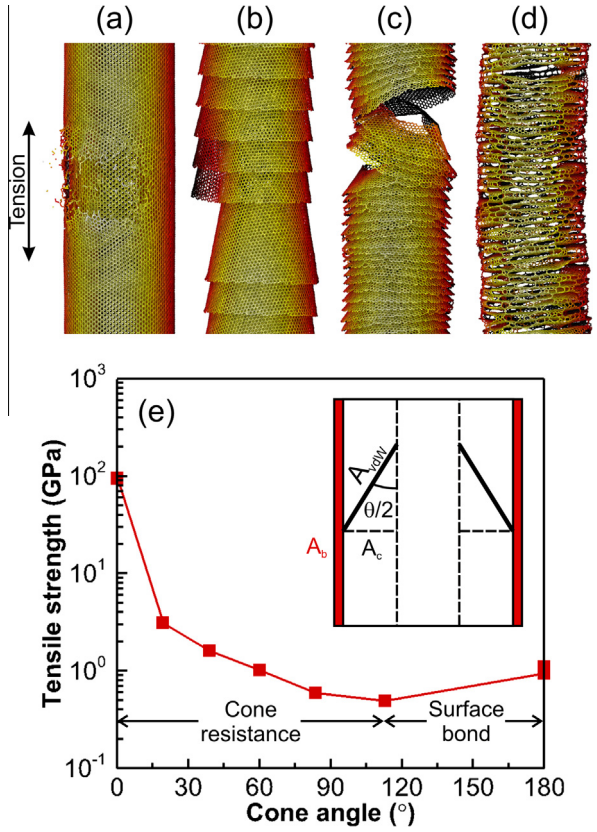

Fig. 6 – Effect of cone structure on tensile strength of CNFs at 300 K. Atomistic snapshots in (a) a MWCNT at 22% deformation and (b) – (d) CNFs with $\theta = 19.2°$, 83.6°, and 180°, respectively, at 16% deformation. (e) Simulated strength vs. cone angle. Note that for MWCNT (0°) and platelet graphite fiber (180°), strengths have been calculated with two different potentials. The data show a transition from cone decohesion and sliding governed by the resistance of weak vdW forces to surface bond strengthening leading to a strength minimum. (A colour version of this figure can be viewed online.)

contrast, the curve obtained for the MWCNT using the AIREBO potential exhibits an inflection point when the fiber yields, Fig. 5b. It has been reported that the cutoff functions in AIREBO potential can overestimate the force required to break a C–C covalent bond. Therefore, we modified this potential by increasing the onset of the interaction cutoff from 1.7 Å to 1.95 Å. However, the stress–strain curve from the modified potential was found to be identical up to the curve inflection, which will correspond to our prediction of strength in the following. Similarly, the stress–strain curve of the platelet-like graphitic fiber using both AIREBO potential and modified AIREBO potential are almost identical with an elastic limit being difficult to distinguish, Fig. 5c. Therefore, for consistency, the strength was also determined by taking the stress at the inflection point.

Furthermore, the atomistic snapshots presented in Fig. 6a–d and the stress–strain curves in Fig. 5a reveal a marked transition of deformation mechanisms from localized brittle fracture to distributed plasticity as the cone angle increases. For $\theta = 0°$, the MWCNT structure is observed to break by the formation and propagation of a transverse crack in the outermost graphene layer, Fig. 6a, leading to a brittle-like behavior. The fracture of CNFs with $\theta < 60°$ is also brittle, but rather results from local sliding and decohesion between cones by a "sword-in-sheath" mechanism [30], Fig. 5b. CNFs with $\theta \geqslant 60°$, Fig. 6c–d, exhibit an increased resistance to the crack propagation and cone decohesion, while plastic deformation becomes increasingly more distributed as θ and the density of surface bonds augment.

The stretching limit of graphitic sp^2 bonds primarily governs the strength of MWCNTs, which only depends on diameter and wall thickness [31]. For cup-stacked CNFs, however, the complex hybrid structure gives rise to additional strengthening mechanisms directly affected by the cone angle. The above deformation mechanisms suggest that, unlike CNTs, the weakest links controlling the strength of cup-stacked CNFs are the interlayer vdW interactions and the surface bonds introduced by thermal treatment, as opposed to the deformation of internal sp^2 bonds in cones. Fig. 6e confirms this conclusion by showing that the tensile strength of CNFs decreases with increasing θ, and increases again between 112.9° and 180°, leading to a minimum in tensile strength at a critical cone angle. Therefore this behavior is indicative of a transition from cone resistance against interlayer sliding to surface bond reinforcement.

To further interpret the minimum of strength, we consider the conical morphology of the CNF core, for which interlayer vdW forces act on an oblique area

$$A_{vdW} = \frac{A_c}{\sin\left(\frac{\theta}{2}\right)} \tag{6}$$

with A_c the cross-section area of core material as schematically illustrated in inset of Fig. 6e. The applied load is distributed between A_{vdW} and the total area of surface bonds A_b. Assuming $f \approx A_b/(A_c + A_b)$ and $1 - f \approx A_c/(A_c + A_b)$ yields a simple expression for the strength of thermally-treated CNFs σ_y such as

$$\sigma_y = f\,\sigma_b + \frac{1-f}{\sin\left(\frac{\theta}{2}\right)}\,\sigma_c, \tag{7}$$

where σ_b and σ_c are the strength of surface bonds and interlayer vdW interactions, respectively. At low angles, $\theta < 60°$, vdW interactions are predominant with little to no surface bonds ($f \ll 1$, Fig. 2h). However, the vdW contribution decreases with increasing θ; for instance, in Fig. 6e, CNF strength is 3 times larger at $\theta = 19.2°$ than at $\theta = 60°$. Therefore, $\sigma_y \approx \sigma_c/\sin\left(\frac{\theta}{2}\right)$, which gives $\sigma_c = 0.523$ GPa by fitting of our MD data for $19.2° \leqslant \theta \leqslant 60°$. For large cone angles, however, the density of surface bonds becomes significant and its contribution is no longer negligible. Using $f = 4.14\%$ and the average tensile strength at $\theta = 180°$ in Eq. (7), we find $\sigma_b = 12.6$ GPa. This analysis therefore emphasizes the significance of strengthening mechanisms from surface bonds in cup-stacked CNFs.

Moreover, it should be pointed out that the tensile strength described in this study is likely different from the stress to failure, because most fibers in Fig. 5a still carry some amount of load at 16% deformation after yielding, which means that little to no surface bonds are broken. The CNF behavior is therefore like a crack problem–the vdW bonding being weak and thus concentrating the applied forces at the ends of the cones where the covalent bonds exist. The fracture stress should therefore presumably depend sensitively on the detailed bonding and its statistical distribution along the CNF length.

4. Conclusions

This study focused on the atomic-scale processes of deformation in cup-stacked CNFs with a wide range of cone angles has shown the strong dependence of mechanical behavior on cone angle in these materials. Our results show evidence for a minimum in tensile strength at a critical cone angle between 112.9° and 180°. We have found that interlayer vdW forces provide the predominant strength contribution at $\theta < 60°$, whereas elastic stiffening and strengthening mechanisms are primarily ascribed to surface bonds, which can attain up to 4.6% of the total volume of fiber when $\theta \geqslant 60°$. We also proposed a model to predict the tensile strength of CNFs as a function of density of surface bonds and cone angle. CNFs made experimentally or available commercially are known to exhibit significant statistical dispersion in failure strength, making accurate predictions of their mechanical behavior difficult for applications. Our findings therefore shed new light on the possible origin for such dispersions, and suggest that the design of high-strength CNFs can be optimized structurally by appropriately tuning the cone angle during synthesis.

Acknowledgments

This work was funded by the Vermont Space Grant Consortium/NASA (Vermont EPSCoR) CAN NNX07AT56A, Dr. Michael Wilder, technical monitor. The computer resources provided by the Vermont Advanced Computing Center (NASA grant NNX06AC88G) are also gratefully acknowledged.

REFERENCES

[1] Tibbetts GG, Lake ML, Strong KL, Rice BP. A review of the fabrication and properties of vapor-grown carbon nanofiber/polymer composites. Composites Sci Tech 2007;67(7–8):1709–18.
[2] Palmeri MJ, Putz KW, Brinson LC. Sacrificial bonds in stacked-cup carbon nanofibers: biomimetic toughening mechanisms for composite systems. ACS Nano 2010;4(7):4256–64.
[3] Barcena J, Coleto J, Zhang SC, Hilmas GE, Fahrenholtz WG. Processing of carbon nanofiber reinforced ZrB2 matrix composites for aerospace applications. Adv Eng Mater 2010;12(7):623–6.
[4] Yoon SH, Park CW, Yang H, Korai Y, Mochida I, Baker RTK, et al. Novel carbon nanofibers of high graphitization as anodic materials for lithium ion secondary batteries. Carbon 2004;42(1):21–32.
[5] Huang CW, Wu YT, Hu CC, Li YY. Textural and electrochemical characterization of porous carbon nanofibers as electrodes for supercapacitors. J Power Sources 2007;172(1):460–7.
[6] Rehammar R, Ghavanini FA, Magnusson R, Kinaret JM, Enoksson P, Arwin H, et al. Electromechanically tunable carbon nanofiber photonic crystal. Nano Lett 2012;13(2):397–401.
[7] Krishnan A, Dujardin E, Treacy MMJ, Hugdahl J, Lynum S, Ebbesen TW. Graphitic cones and the nucleation of curved carbon surfaces. Nature 1997;388(6641):451–4.
[8] Tibbetts GG, Beetz JCP. Mechanical properties of vapour-grown carbon fibres. J Phys D: Appl Phys 1987;20(3):292.
[9] Jacobsen RL, Tritt TM, Guth JR, Ehrlich AC, Gillespie DJ. Mechanical properties of vapor-grown carbon fiber. Carbon 1995;33(9):1217–21.
[10] Ozkan T, Naraghi M, Chasiotis I. Mechanical properties of vapor grown carbon nanofibers. Carbon 2010;48(1):239–44.

[11] Lawrence JG, Berhan LM, Nadarajah A. Elastic properties and morphology of individual carbon nanofibers. ACS Nano 2008;2(6):1230–6.
[12] Beese AM, Papkov D, Li S, Dzenis Y, Espinosa HD. In situ transmission electron microscope tensile testing reveals structure–property relationships in carbon nanofibers. Carbon 2013;60:246–53.
[13] Ekşioğlu B, Nadarajah A. Structural analysis of conical carbon nanofibers. Carbon 2006;44(2):360–73.
[14] Wei C, Srivastava D. Nanomechanics of carbon nanofibers: structural and elastic properties. Appl Phys Lett 2004;85(12):2208–10.
[15] Uchida T, Anderson D, Minus M, Kumar S. Morphology and modulus of vapor grown carbon nano fibers. J Mater Sci 2006;41(18):5851–6.
[16] Plimpton S. Fast parallel algorithms for short-range molecular dynamics. J Comp Phys 1995;117:1–19.
[17] Brenner DW, Shenderova OA, Harrison JA, Stuart SJ, Ni B, Sinnott SB. A second-generation reactive empirical bond order (REBO) potential energy expression for hydrocarbons. J Phys Cond Matter 2002;14(4):783.
[18] Belytschko T, Xiao SP, Schatz GC, Ruoff RS. Atomistic simulations of nanotube fracture. Phys Rev B 2002;65(23):235430.
[19] Jeong BW, Lim JK, Sinnott SB. Tensile mechanical behavior of hollow and filled carbon nanotubes under tension or combined tension-torsion. Appl Phys Lett 2007;90(2):023102–23103.
[20] Gu J, Sansoz F. An atomistic simulation study of the mechanisms and kinetics of surface bond strengthening in thermally-treated cone-stacked carbon nanofibers. Carbon 2013;56:351–7.
[21] Stukowski A. Visualization and analysis of atomistic simulation data with OVITO-the Open Visualization Tool. Mod Simul Mater Sci Eng 2010;18(1).
[22] Xia ZH, Guduru PR, Curtin WA. Enhancing mechanical properties of multiwall carbon nanotubes via sp^3 interwall bridging. Phys Rev Lett 2007;98(24):245501.
[23] Peng B, Locascio M, Zapol P, Li S, Mielke SL, Schatz GC, et al. Measurements of near-ultimate strength for multiwalled carbon nanotubes and irradiation-induced crosslinking improvements. Nat Nano 2008;3(10):626–31.
[24] Zhang YY, Wang CM, Cheng Y, Xiang Y. Mechanical properties of bilayer graphene sheets coupled by sp^3 bonding. Carbon 2011;49(13):4511–7.
[25] Endo M, Kim YA, Hayashi T, Fukai Y, Oshida K, Terrones M, et al. Structural characterization of cup-stacked-type nanofibers with an entirely hollow core. Appl Phys Lett 2002;80(7):1267–9.
[26] Endo M, Kim YA, Hayashi T, Yanagisawa T, Muramatsu H, Ezaka M, et al. Microstructural changes induced in “stacked cup” carbon nanofibers by heat treatment. Carbon 2003;41(10):1941–7.
[27] Feng J, Qi L, Huang JY, Li J. Geometric and electronic structure of graphene bilayer edges. Phys Rev B 2009;80(16):165407.
[28] Liu Z, Suenaga K, Harris PJF, Iijima S. Open and closed edges of graphene layers. Phys Rev Lett 2009;102(1):015501.
[29] Shen YK, Wu HA. Interlayer shear effect on multilayer graphene subjected to bending. Appl Phys Lett 2012;100(10). 101909-3.
[30] Yu MF, Lourie O, Dyer MJ, Moloni K, Kelly TF, Ruoff RS. Strength and breaking mechanism of multiwalled carbon nanotubes under tensile load. Science 2000;287(5453):637–40.
[31] Natsuki T, Tantrakarn K, Endo M. Effects of carbon nanotube structures on mechanical properties. Appl Phys A 2004;79(1):117–24.